Advanced Study of Switchable Spin Crossover Compounds

Gavin Craig

ADVANCED STUDY OF SWITCHABLE SPIN CROSSOVER COMPOUNDS

Universitat de Barcelona

Facultat de Química

Departament de Química Inorgànica

Programa de Doctorat: Química Inorgànica Molecular

Grup de Magnetisme i Molècules Funcionals

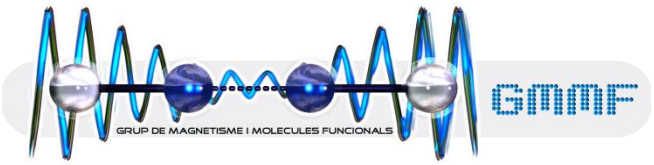

Gavin Craig

Director: Dr. Guillem Aromí Bedmar, Departament de Química Inorgànica

Tutor: Dr. Santiago Alvarez Reverter, Departament de Química Inorgànica

Contents

Chapter 3: Towards novel polypyrazolyl ligands for SCO systems

3.0 Introduction

Ligands containing pyrazolyl rings have been successfully used in many areas of coordination chemistry.[1, 2] The possibility of coordinating both N-donor atoms in the pyrazolyl ring to separate metal centres, bringing them into close proximity, confers unusual chemical properties upon their complexes. This has been exploited to synthesise compounds which range from water oxidation catalysts[3-5] to luminescent clusters of the precious metals,[6, 7] and through to high nuclearity clusters of interest in the field of molecular magnetism.[8-12] Within this latter field, advantage has been taken of the relative ease with which the N atom may be deprotonated, and with which the pyrazolyl ring may be functionalised at the C atoms. Thus, modification at the 3- and 5- positions influences the sterics of the ligating species, while appending functional groups at the 4- position has a more direct effect on the ligand's electronic properties on coordination (Scheme 3.1).[13]

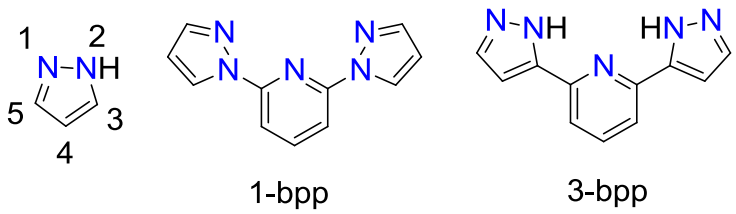

Scheme 3.1: A view of the pyrazole ring (left); and the two regio-isomers of the bis(pyrazolyl)pyridine ligands, 1-bpp (centre) and 3-bpp (right).

As discussed in Chapter 1, an important part of SCO research has focused on systems derived from polypyrazolyl ligands of the type bis(pyrazol-x-yl)pyridine (x =1 or 3: 1-bpp or 3-bpp, respectively).[14, 15] These ligands tend to coordinate to a single Fe(II) core, leading to a FeN_6 coordination sphere in a cation of the formula $[Fe(x\text{-bpp})_2]^{2+}$, the rest of the components associated with it depending on synthetic details. In the case of systems containing derivatives of the 1-bpp ligand, examples may be found of functionalisation at every available point of the pyrazolyl ring,[15-18] and a selection of groups appended to the 4-position of the pyridyl ring,[19-21] leading to over 130 reported crystal structures in the CSD.

This depth of variety contrasts with that of 3-bpp where, prior to this thesis, no synthetic derivative had been employed in the development of SCO systems. This difference was commented upon in a recent review by Olguín et al. where the complete lack of an SCO active Fe(II) complex based on a derivative of 3-bpp was ascribed to synthetic difficulties.[22] Instead, the majority of research carried out on this regio-isomer has studied the extreme sensitivity of $[Fe(3\text{-bpp})_2]^{2+}$ compounds to the charge-balancing anion[23-26] and, especially, the degree of hydration of the sample.[27-30] In the latter case, one of the more remarkable examples is the system $[Fe(3\text{-bpp})_2](CF_3SO_3)_2 \cdot xH_2O$ (x = 1 or 3).[31, 32] Here, two water molecules may be removed from the HS trihydrate salt, leading to a monohydrate which displays an abrupt SCO in the cooling mode, a two-step SCO in the heating mode, and a hysteresis loop which measures over 140 K at its widest point. As with other compounds in this series, the rationalisation of the observed magnetic properties is hindered by the lack of structural data in the form of a single crystal structure. In those cases where the crystal structure has been resolved, the most recurrent packing motif is found to be that of the "terpyridine embrace", where cross-shaped cations interact through the overlap of the ligand wings and are reinforced by the interaction of a terminal pyrazolyl C-H group with the π-electron density that resides on the face of a neighbouring pyrazolyl ring.[33-35] It could be postulated that by modifying the wings of the 3-bpp ligand, to include further aromatic rings and additional hydrogen donor groups, that the array of intermolecular interactions could be improved, and increase the possibility of crystallising mononuclear Fe(II) compounds of 3-bpp moieties.

In this Chapter, the magnetic properties of a novel $[Fe(3\text{-bpp})_2]^{2+}$ compound are described, as well as the crystal structures at high and low temperature. An elegant way of preparing derivatives of 3-bpp and other polypyrazolyl ligands is outlined, based on previous research in our group. The dual use of these polytopic ligands is discussed: firstly, the coordinative flexibility of the donor moieties has given access to compounds that again justify the interest in employing polypyrazolyl ligands as the skeleton of metal clusters. Secondly, the anticipated augmentation of the supramolecular chemistry associated with these ligands is observed in the crystal structure of the novel ligand 2,6-bis(5-(2-hydroxyphenyl)-pyrazol-3-yl)pyridine, in which the distal phenol rings participate in hydrogen bonding motifs, at the same time maintaining the π-π interactions of the central 3-bpp core.

3.1 Synthesis

The synthesis of the compound $[Fe(3\text{-bpp})_2](ClO_4)_2 \cdot 1.75\ C_3H_6O \cdot 1.5\ C_4H_{10}O$ (**i**) involves the aerobic reaction of $Fe(ClO_4)_2 \cdot xH_2O$ with two moles of the ligand bis(pyrazol-3-yl)-pyridine in acetone at room temperature. Ascorbic acid was used as an anti-oxidant, to maintain the iron centres in the divalent state. Layering the reaction solvent with diethyl ether yielded crystals of suitable quality for single crystal X-ray diffraction studies after two to three days. Removal of the orange crystals from the solvent led to the rapid degradation of the sample, and a loss of crystallinity. Therefore, the crystals were covered in a drop of Paratone oil and mounted as quickly as possible in the diffractometer, in order to collect data. This sensitivity also affected the magnetic measurements, where a powder was used, rather than the crystal sample.

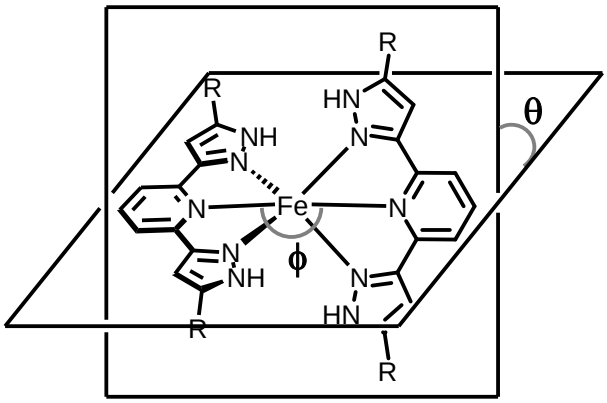

Figure 3.1: A view of the coordination of two 3-bpp type ligands to an Fe centre, with the parameters θ and Φ illustrated.

3.2 Definitions of the structural parameters $\theta, \Phi, \Sigma, \Theta$

Over the course of the thesis, reference will be made to four structural parameters: θ, Φ, Σ, Θ. Their full significance and bearing on the spin state of the Fe(II) complexes will be discussed in Chapter 9, although it is useful to set out their definition before they are mentioned in the following structural descriptions. The first two parameters were devised expressly to characterise the distortion in complexes that consist of two planar tri-dentate ligands coordinated to a metal centre in a *mer*- fashion. Because these ligands usually coordinate in a pseudo-perpendicular way, θ has been used to measure the angle formed by the least squares planes defined by the chelating ligands (Figure 3.1).[36, 37] This involved selecting all of the atoms in a given ligand, including hydrogen atoms, and calculating the least squares plane in the program Mercury. Once both are defined, the

angle is then easily obtained. The second parameter, Φ, corresponds to the trans N-Fe-N angle formed by the coordination of the central pyridyl rings to the Fe(II) ion.[37] Therefore, the ideal values of these parameters are 90° and 180°, respectively. Both parameters serve to characterise how the two coordinating ligands are oriented with respect to each other, which in turn is the defining factor in the molecular shape of the cations.[14] Large variation of these parameters from their ideal values has previously been interpreted as a result of the Jahn-Teller effect.[38]

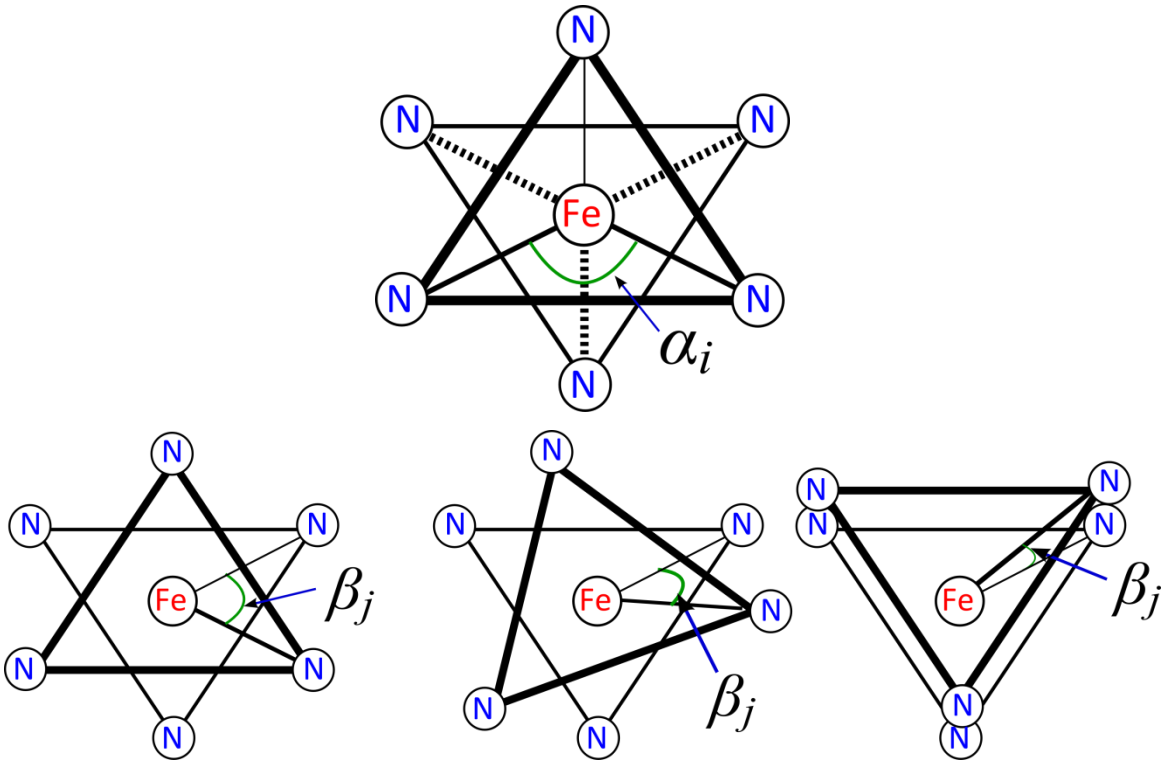

Figure 3.2: (top) An illustration of the bite angles α that are used in the sum of Σ. (bottom) A view of the angle β, which is used to evaluate Θ, and how it varies as the ideal octahedron is distorted towards a trigonal primatic symmetry.

In contrast, the parameters Σ and Θ are significant of a more local distortion concerning the Fe(II) ion and its immediate coordination sphere (Figure 3.2).[39, 40] The bite angle of the tri-dentate ligands leads to a particular deformation around the metal centre, which is measured by Σ as the sum of the deviation away from 90° of the twelve possible *cis*-N-Fe-N bite angles. As such, the value for an ideal octahedron is $\Sigma = 0$, so that the higher the value, the greater the distortion. The formula used for the calculation is the following:[41]

$$\Sigma = \sum_{i=1}^{12} |90 - \alpha_i|$$

With the value of Θ, a measure of the twist away from perfect octahedral symmetry, O_h, towards a trigonal prismatic symmetry, D_{3h}, is obtained. In an ideal octahedron, there are 8 threefold symmetry axis, which pass through the centre of the triangular faces of the polyhedron in such a way that the angle formed between the *cis*- vertices on projection of the faces measures 60° (Figure 3.2, left). As the octahedron twists towards towards D_{3h}, these angles vary from 60°, before eventually reaching 0 in the fully eclipsed arrangement. There are 24 such N-Fe-N angles, and Θ is the sum of their deviation from 60°:[41]

$$\Theta = \sum_{j=1}^{24} |60 - \beta_j|$$

To perform this calculation, the program Olex 2.0[42] was used. First, the user selects the central ion of the octahedron, and then in a clockwise fashion selects the six donor atoms in order as they appear on the screen. By typing the command "sel", the program then executes the measurement, and provides the value. Previous analyses have demonstrated that complexes in the HS state are associated with greater flexibility, allowing them to reach higher degrees of distortion than LS systems. In fact, in one set of systems, extreme distortion of the HS state was suggested to trap the compound in a HS state, causing a barrier to its possible transition to the singlet state.[37]

3.3 Single crystal X-ray diffraction study

Compound **i** crystallises in the monoclinic space group C2/c, and the unit cell contains eight $[Fe(3\text{-bpp})_2]^{2+}$ cations, with two in the asymmetric unit. The charge of the complex is balanced by two perchlorate anions per cation, while the asymmetric unit is completed by three and a half lattice molecules of acetone and three of ether. The cations display the coordination typical of 3-bpp, consisting of two neutral 3-bpp ligands binding to the Fe(II) through their three central nitrogen atoms, leading to a pseudo-octahedral geometry and an FeN_6 coordination sphere (Figure 3.3). The crystal structure of **i** was initially elucidated at 250 K, before a complementary structure was resolved at 90 K, which was found to be iso-structural. Table 3.1 compiles the data concerning data collection and resolution. The twelve Fe-N bond lengths – six for each cation – lie in the range (250/90 K) 2.121(3)/2.031(3) to 2.209(3)/2.082(4) Å, with an average value of

Compound	**i**			
T/K	250(2)		90(2)	
crystal system	Monoclinic		Monoclinic	
space group	C2/c		C2/c	
a/Å	46.029(2)		45.425(5)	
b/Å	14.206(1)		14.224(1)	
c/Å	26.278(1)		25.685(3)	
α/°	90		90	
β/°	102.82(1)		104.24(1)	
γ/°	90		90	
V/Å^3	16754.2(15)		16085(3)	
μ/mm^{-1}	0.697		0.726	
reflections collected	16476		16445	
R1 (all data)	0.0861		0.0955	
wR2 (all)	0.21025		0.1984	
S	1.031		1.048	
	Fe1	Fe2	Fe1	Fe2
av. Fe-N/Å	2.168	2.169	2.057	2.057
octahedral volume/Å^3	12.397	12.533	10.891	10.940
Σ/°	147.69	145.15	122.60	120.51
Φ/°	168.91(2)	174.65(2)	171.84(2)	174.42(2)
θ/°	88.58	87.62	89.60	88.77
Θ/°	487.61	476.56	403.37	394.97

Table 3.1: Crystallographic data and selected structural parameters for compound **i**.

2.168/2.057 Å while the 250 K value is typical for an Fe(II) system in the HS state, the value at 90 K is indicative of an incomplete transition to the LS state.[43] The average bond length at low temperature is thus due to a weighted contribution of the proportion of HS and LS centres in the cation sites, and is in fact the same for both cations, indicative of a lack of long-range ordering to the spin state distribution. The two chelating species lie in two different planes and the structure of the ligand imposes restrictions on the possible bite angle, allowing the use of the four parameters defined in Section 3.2.[44, 45] Upon cooling from 250 to 90 K, the average values of θ and Φ increase from 88.1° and 172.3°

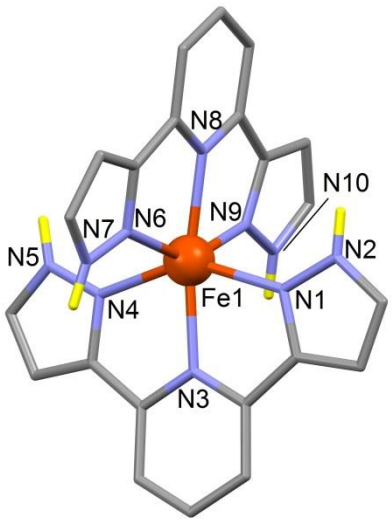

	Bond length/Å	
Bond	250 K	90 K
Fe1-N3	2.134(3)	2.028(4)
Fe1-N8	2.130(3)	2.024(4)
Fe1-N1	2.189(3)	2.072(4)
Fe1-N4	2.169(3)	2.060(4)
Fe1-N6	2.198(3)	2.082(4)
Fe1-N9	2.187(3)	2.078(5)
Average	2.166	2.057

Figure 3.3 and Table 3.2: A view of one of the $[Fe(3\text{-bpp})_2]^{2+}$ cations in **i**. Hydrogen atoms are omitted for clarity, except those bonded to nitrogen. The Fe-N bond lengths at 250 and 90 K are detailed in the table.

to 89.2° and 173.1°, respectively, indicative of an increased regularity in shape of the cation, resulting from the SCO process. The decrease in the values of Σ and Θ, from 146.42° to 121.56°, and from 482.09° to 399.17°, respectively, amounts to a more regular coordination octahedron in the LS state than in the HS state.

With its combination of hydrogen bond donors and planar nature, the ligand 3-bpp could be expected to induce significant intermolecular interactions between the cations, typically in the form of the so-called "terpyridine embrace".[33-35] However, **i** does not display this packing motif, a more detailed description of which will be given in the

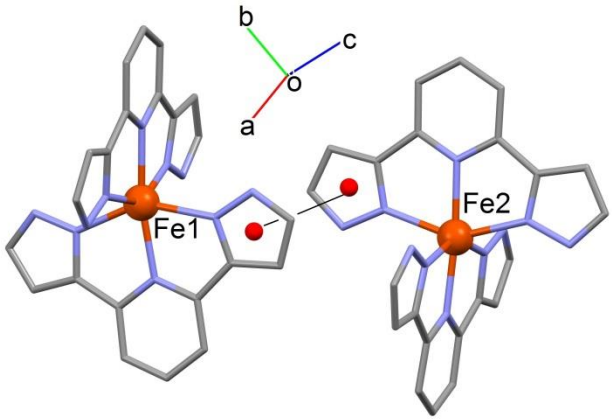

Figure 3.4: A view of the $\pi\cdots\pi$ contact between the two nearest neighbour $[Fe(3\text{-bpp})_2]^{2+}$ cations in **i**. Hydrogen atoms are omitted for clarity, and the contact is shown between the centroids of the relevant pyrazolyl rings.

following Chapter. The supramolecular connectivity of these $[Fe(3\text{-}bpp)_2]^{2+}$ complexes is largely mediated by interactions through the lattice solvent molecules and anions, rather than direct contact between the cations. Indeed, despite the presence of six aromatic rings in each cation, there is only one $\pi\cdots\pi$ contact, which arises between the distal pyrazolyl rings of nearest neighbour cations (Figure 3.4), measuring 3.906(3)/3.756(3) Å between the centroids of the rings. This interaction is also that which brings the Fe(II) atoms into closest proximity, with an inter-iron distance of 8.645(1)/8.458(1) Å. Considering a pair of nearest neighbour cations Fe1 and Fe2, there is then a C-H$\cdots\pi$ interaction with the lattice ether molecules, which serves to link one pair of Fe1Fe2 cations with another (Figure 3.5). Though this relationship between the cations and the ether molecules helps to hold the structure together, it prevents the tighter arrangement observed in the "terpy embrace" by impeding a greater degree of $\pi\cdots\pi$ overlap. The interaction strengthens on transition to the LS state, with the C-H$\cdots$centroid distance decreasing (3.563(8)/3.442(8) Å).

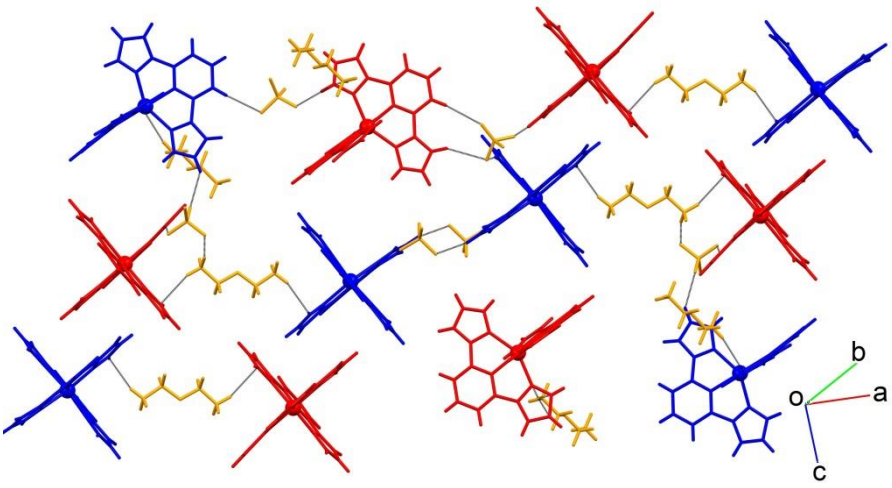

Figure 3.5: The arrangement in 2D of the cations within **i**. The two crystallographically distinct cations are shown either in red or blue, with the C-H$\cdots\pi$ or C-H$\cdots$anion contacts shown by lines.

These $\pi\cdots\pi$ and C-H$\cdots\pi$ interactions are the determining intermolecular contacts in the crystal lattice. While the pyrazolyl rings of each ligand partake in hydrogen bonding motifs – one ligand to an acetone molecule and a perchlorate anion, the other to a diethyl ether molecule and another perchlorate anion – the subsequent hydrogen bonds are not sufficient for a strong contact to other cations, because they are primarily conducted through C-H bonds (Figure 3.6).

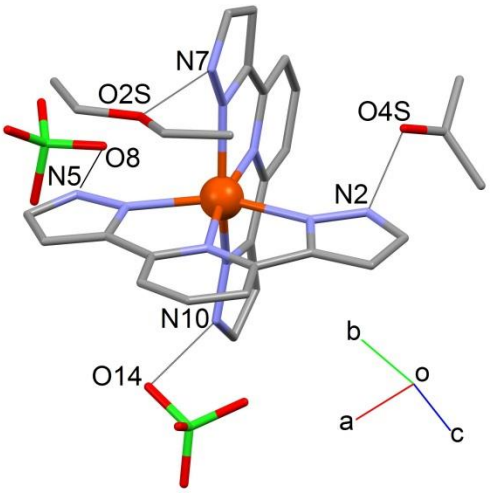

	Bond length/Å	
Bond	250 K	90 K
N2-H2···O4S	2.792(6)	2.756(7)
N5-H5···O8	3.083(7)	2.908(6)
N7-H7···O2S	2.842(5)	2.798(5)
N10-H10···O14	3.032(7)	3.134(8)

Figure 3.6 and Table 3.3: A representation of the hydrogen bonding motifs in which the pyrazolyl rings of the 3-bpp ligand participate for one of the cations of **i**. Hydrogen atoms have been omitted for clarity.

3.4 Magnetic properties

The crystals of **i** were found to degrade quickly when they were removed from the solvent system used for their formation, leading to a rapid loss in crystallinity. Therefore, it was only possible to measure the magnetic properties of a dry powder. The measurement was then executed under an applied field of 5 kG, in a temperature range of 5-300 K, and is represented as the molar magnetic susceptibility product, χT, *vs.* the temperature, T, in Figure 3.7. At 300 K, χT = 3.21 $cm^3mol^{-1}K$, corresponding to Fe(II) in a HS state (χT = 3.00 $cm^3mol^{-1}K$ for S = 2 and g = 2.0).[46] Lowering the temperature at a rate of 1 $Kmin^{-1}$ causes an immediate decrease in the value of χT, which continues in a gradual form until below 100 K, where the magnetic response enters a plateau corresponding to a value of χT = 0.44 $cm^3mol^{-1}K$. This behaviour is consistent with a gradual, incomplete SCO process. Taking $T_{1/2}$ as the temperature at which the observed SCO process is half-way complete, then **i** has $T_{1/2}$ = 220 K. The nature of the transition over a wide temperature range is indicative of low levels of cooperativity within the system,[47] while the decrease in χT below 20 K is brought about by zero field splitting effects in those Fe(II) ions which remain in the HS state.[48] As a means of comparison between the powder's magnetic properties and those of the crystal sample, the χT values of at the temperatures of the crystal structures may be contrasted with the average Fe-N bond lengths determined under the same conditions. The observed values of χT at 250 and 90 K are 2.778 and 0.45 $cm^3mol^{-1}K$, which correspond to HS fractions of 87 % and 14 %,

respectively. However, the average bond lengths at these temperatures are 2.168 and 2.087 Å: closer to HS populations of 100 % and 50 %, respectively, when compared to the average HS and LS values taken from compounds found in the literature. This suggests that the magnetic properties of the crystal form of **i** differ significantly from those of the bulk powder.

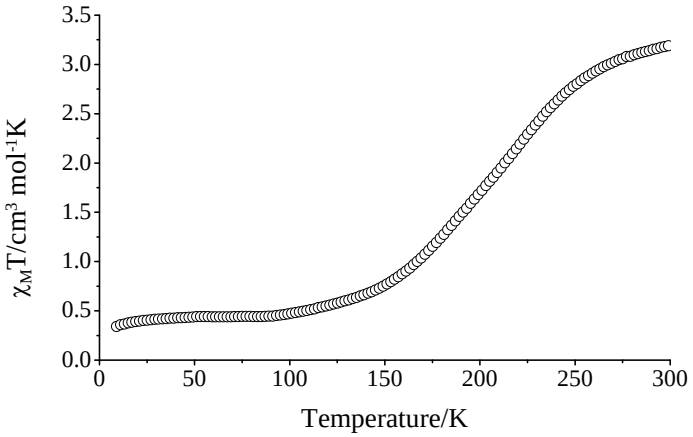

Figure 3.7: χT *vs.* T for a dried powder sample of **i** in the temperature range 300 to 5 K, measured at a rate of 1 $Kmin^{-1}$.

3.5 Differential Scanning Calorimetry

The energetics of the gradual transition of **i** between the spin states were investigated using DSC in the heating mode. Figure 3.8 displays the raw heat flow data *vs.* temperature for the SCO process, which is associated with a broad anomaly centred around 190 K. By subtracting a normal heat capacity curve from the heat capacity measurement, the excess heat capacity, ΔC_P, was derived (Figure 3.8, right). Integration of ΔC_P over T[49] yields the value of the excess enthalpy, ΔH, which in the case of **i** was found to be 5.58 $kJmol^{-1}$. Alternatively, integration over ln$T$ leads to the value of excess entropy, ΔS = 28.3 $Jmol^{-1}K^{-1}$. This value is higher than that predicted for the change of spin state (Rln(5) = 13.4 $Jmol^{-1}K^{-1}$), though it lies below the range expected in the case of highly cooperative systems (ΔS > 50 $Jmol^{-1}K^{-1}$).[50] As such, it is consistent with the SCO process as observed by SQUID magnetometry. Although the temperature at which ΔC_P shows its maximum (190 K) is different to the value of $T_{1/2}$, this effect can be attributed to the different speed of temperature change, which was 10 $Kmin^{-1}$ in the case of the DSC measurements.

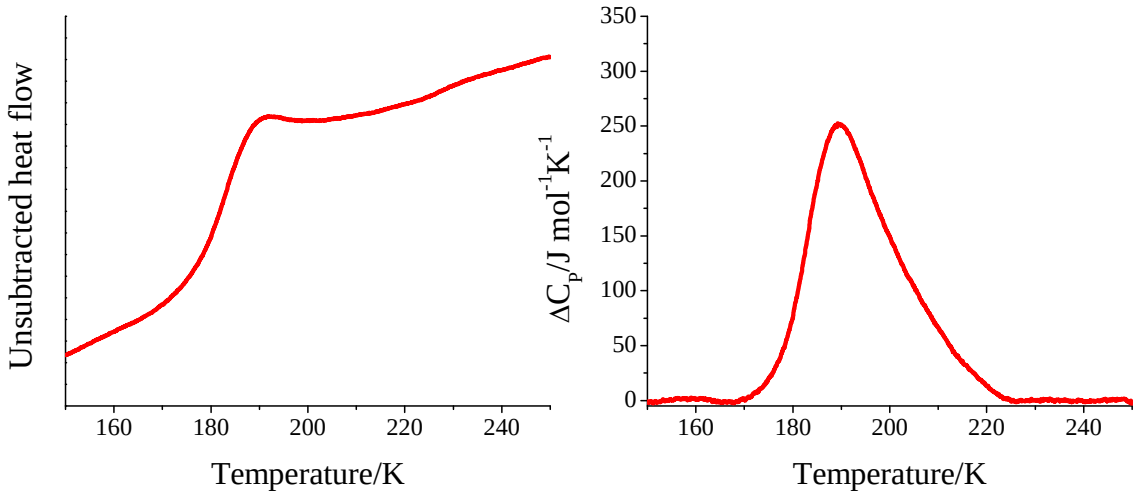

Figure 3.8: (left) The unsubtracted heat flow in the heating mode for compound **i** in the temperature range 250 to 150 K . (right) The excess heat capacity, ΔC_P, yielded by the heat flow experiments.

3.6 Development of polypyrazolyl derivatives

The scarcity of crystal structures associated with $[Fe(3\text{-bpp})_2]^{2+}$ systems led to the proposal that by amplifying the functionality of the ligand, the formation of single crystals could be encouraged. Subsequent study of magnetic properties could then be related to the way in which spin-active lattice components are maintained in contact through entities in the crystal structure, whether directly through the cations themselves, or through solvents or anions. This line of research therefore required suitable design of ligands to be able to meet these objectives. The strategy employed to obtain polypyrazolyl ligands consisted in the ring-closing reaction of β-diketone groups through reaction with hydrazine monohydrate.[51] For this purpose, use was made of bis-β-diketone ligands that had been synthesised previously in our group.[52] These ligands had been designed with the goal of directing the construction of metal clusters, moving away from serendipitous assembly[53] towards a more controlled model, by combining various functional groups at specific points in the backbone of the chelating species. This approach had successfully yielded clusters which displayed site-selectivity in their metal composition,[54] and compounds where the covalent spine provided by the ligand brought together two tetranuclear spin entities within the same molecule.[55, 56]

To undertake this synthetic methodology, the corresponding bis-β-diketone ligand was prepared via Claisen condensation, which consists of a deprotonated methylketone attacking the relevant ester that is to provide the core of the molecule (Figure 3.9). Once

obtained, the reflux of the diketone ligand with hydrazine monohydrate led to the precipitation of the novel polypyrazolyl ligands 2,6-bis(5-(2-hydroxyphenyl)-pyrazol-3-yl)pyridine (H_4L), 2,6-bis(5-(2-methoxyphenyl)-pyrazol-3-yl)pyridine (H_2L1), and 2,6-bis(5-(2-hydroxyphenyl)-pyrazol-3-yl)benzene (H_4L2).

The formation of pyrazolyl rings on either side of the central pyridyl ring in the cases of H_4L and H_2L1 mean that they can therefore be considered as functionalised derivatives of the common SCO ligand 3-bpp. Although a small number of derivatives of 3-bpp had been synthesised using Claisen condensation to functionalise the molecule at the pyrazole C atoms,[57-59] none of the thus obtained ligands had been used in spin crossover research. Rather, a preference had been shown for derivatives of the regio-isomer bis(pyrazol-1-yl)-pyridine, 1-bpp.

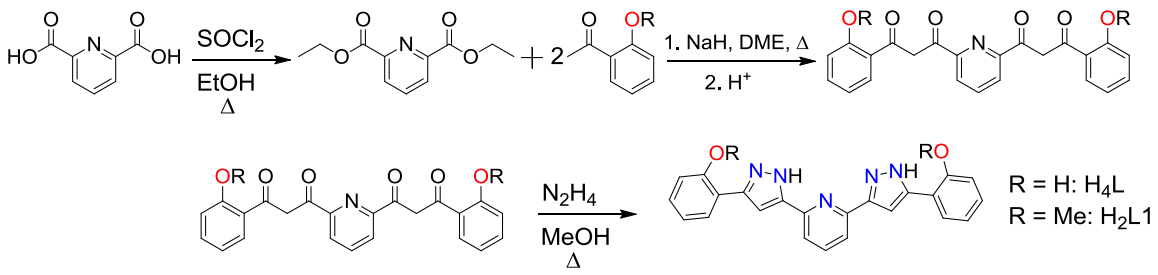

Figure 3.9: Synthesis of ligands H_4L and H_2L1.

As well as the design and synthesis of ligands based around a pyridyl core, this flexible approach allowed the ligand H_4L2 to be obtained. An analogous procedure to that followed for H_4L was employed, differentiating in the use of 1,3-bis(3-oxo-3-(2-hydroxyphenyl)-propionyl)benzene[60] as the starting bis-β-diketone (Figure 3.10).

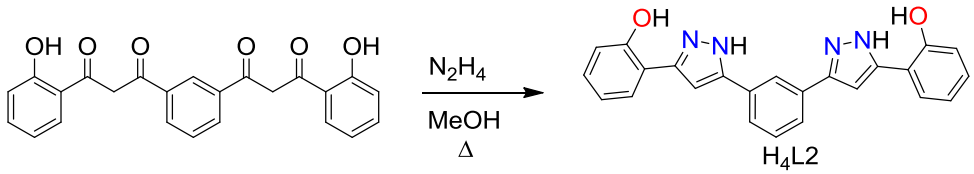

Figure 3.10: Synthesis of the ligand H_4L2.

3.7 Cluster coordination chemistry of the polypyrazolyl ligands

The disposition of the donor atoms in both H_4L and H_4L2 has led to the synthesis of several novel cluster compounds which, although not the focus of this thesis, are of interest in the field of molecular magnetism. The proximity of the heteroatoms within the

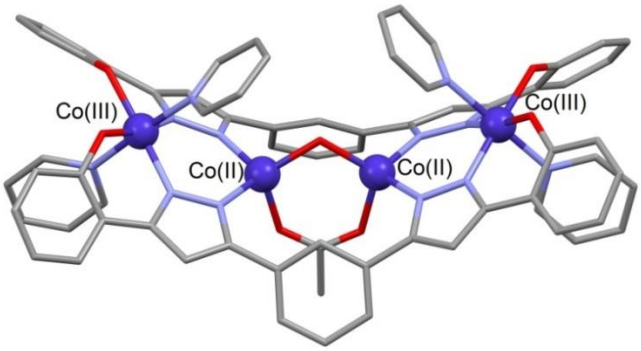

Figure 3.11: A view of $[Co_4(L2)_2(OAc)(OH)(py)_4]$, where the metal atoms and their oxidation states are labelled. Hydrogen atoms have been omitted for clarity, oxygen atoms are shown in red, and nitrogen in light blue.

chelating species allows the polynucleating ligand to coordinate transition metal atoms in such a way that, in the case of H_4L2, linear topologies may be accessed, as prototypes for molecular wires.[61-63] Figure 3.11 shows the crystal structure of the compound $[Co_4(L2)_2(OAc)(OH)(py)_4]$, which forms half of a pair of mixed valence complexes more fully described in Appendix A4. It was found that the bridge between the paramagnetic Co(II) ions could be varied, depending on the reaction conditions. Thus the interaction between these tetrahedral cobalt centres could be studied as a function of the exchange pathway.

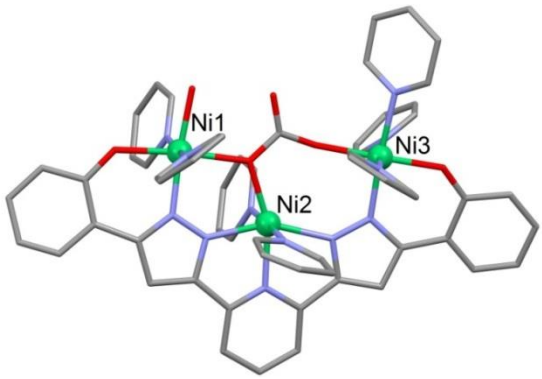

Figure 3.12: A view of the neutral molecule $[Ni_3(L)(CO_3)(H_2O)(py)_7]$. The hydrogen atoms have been omitted for clarity, oxygen atoms are shown in red, and the nitrogen atoms in light blue.

The ligand H_4L has given rise to a host of magnetically interesting cluster complexes, the structures of which are a direct consequence of the design of the polypyrazolyl species. In the compound $[Ni_3(L)(CO_3)(H_2O)(py)_7]$ (see Appendix A8), the coordination of three Ni(II) ions – one in the central coordination pocket to the pyridyl ring, the remaining two to the distal deprotonated pyrazolyl and phenol rings – induced an unusual

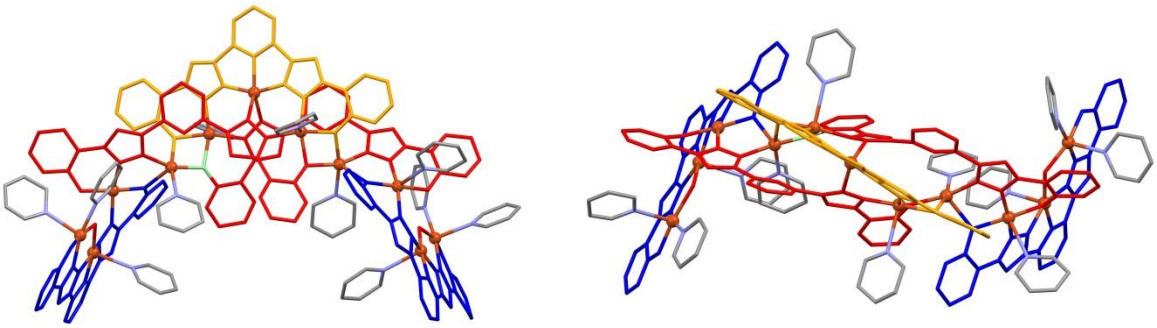

Figure 3.13: Representation of the complex $[Cu_{11}L_5(OH)_2(py)_{12}]$ with the metal atoms in ball and stick mode. The ligands are coloured depending on their coordination mode, and hydrogen atoms are omitted for clarity.

scalene triangular arrangement of the transition metal ions (Figure 3.12). The magnetic properties of this complex were rationalised with emphasis on the role played by an intermolecular hydrogen bond, in which the coordinated H_2O molecules participate. The capability of the ligand to provide different coordination modes is due to the diverse nature of the different donor atoms and the possibility of modulating its coordination by varying the type of base used. Using a strong base like NaH, the ligand was fully deprotonated, and formed a Cu_{11} complex ($[Cu_{11}L_5(OH)_2(py)_{12}]$) in which it chelates the Cu(II) ions in three different ways (Figure 3.13).

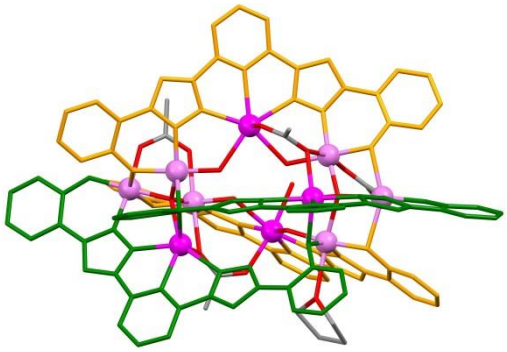

Figure 3.14: Representation of the complex $[Mn_{10}O_2(OH)_4(OAc)_4L_2(HL)_2(thf)(H_2O)_2]$ where the ligands are colour coded for unique coordination modes. The Mn(II) ions are shown in magenta, and the Mn(III) ions in violet.

The sensitivity of this ligand to the exact reaction conditions was also demonstrated by a series of manganese cluster compounds (Appendices A3 and A5), where it was found that control of certain synthetic parameters could lead from a tetranuclear manganese compound through to a Mn_{14} cluster that was the assembly of two well-defined Mn_7

clusters: a key objective in the study of molecular cluster pairs (MCPs).[64] Figure 3.14 shows the Mn_{10} compound ($[Mn_{10}O_2(OH)_4(OAc)_4L_2(HL)_2(thf)(H_2O)_2]$) from this family.

3.8 Crystal structure of H_4L

The crystal structure of the ligand H_4L is shown in Figure 3.15, and the details of the structure resolution are given in Table 3.4. As expected, the molecule consists of 2 phenolpyrazolyl groups linked to a central pyridine ring through both of its *meta* positions. The compound crystallises in the space group $P2_1/c$ and so contains four molecules in the unit cell.

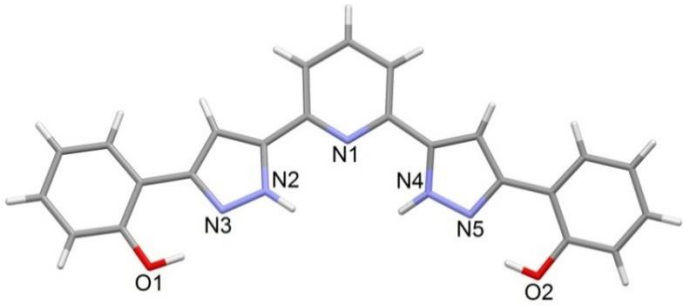

Figure 3.15: A Mercury view of the molecular structure of the ligand H_4L. The heteroatoms are labelled, with hydrogen atoms in light grey and carbon atoms in a darker grey.

The crystal structure also demonstrates the potential for intermolecular interactions that exists within H_4L, the purpose for which it was designed. Both the pyrazolyl and phenol rings participate in hydrogen bonding motifs, and π-π stacking. The ligand is almost co-planar, due to the formation of intramolecular H-bonds between the non-protonated pyrazolyl N atoms and the O atoms of the distal phenol rings. This interaction measures 2.587(2) and 2.630(1) Å for O2-H2B···N5 and O1-H1B···N3, respectively. The torsion angles that are formed by N1-C14-C15-N4 and N1-C10-C9-N2 are 13.53° and 4.63°, respectively, demonstrating the near coplanar nature of the H_4L molecule. The phenol ring and the remaining N atom in the pyrazolyl ring then participate in intermolecular H-bonds with neighbouring molecules of H_4L (Figure 3.16), linking the ligands together in chains (N2-H2···O1 = 2.843(2) Å, and N4-H4···O2 = 2.779(3) Å).

Further, H_4L displays π-π stacking interactions, which link these chains together (Figure 3.16). The core of the ligand participates in this contact, with a distance of 3.553(1) Å between the centroids of the pyridyl rings. The crystal structure therefore demonstrates

Compound	H_4L
Empirical formula	$C_{23}H_{17}N_5O_2$
T/K	100(2)
crystal system	Monoclinic
space group	$P2_1/c$
a/Å	13.173(2)
b/Å	13.384(2)
c/Å	11.211(2)
α/°	90
β/°	110.93(2)
γ/°	90
V/Å^3	1846.2(5)
μ/mm^{-1}	0.095
R1 (all data)	0.0655
wR2 (all)	0.1498
S	1.041

Table 3.4: Crystallographic data and selected structural parameters for compound H_4L.

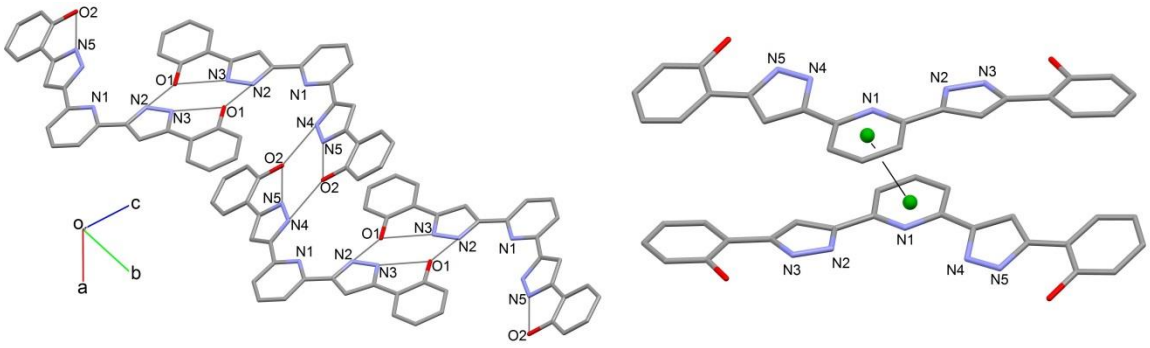

Figure 3.16: (left) A representation of the intermolecular hydrogen bonds which join the molecules of H_4L together into chains. (right) The $\pi\cdots\pi$ contacts between the pyridyl rings.

the capability of H_4L to foment intermolecular interactions, particularly through the distal phenol rings, which represent the additional functionality when compared to 3-bpp.

3.9 Concluding remarks

A mononuclear Fe(II) compound displaying SCO has been synthesised with the ligand 3-bpp. While the crystal structure obtained represents the first in this family of compounds

to contain the perchlorate anion, the overall level of intermolecular interactions is weak, and the system does not crystallise in the previously observed terpyridine embrace. The resulting SCO is poorly cooperative, and incomplete, falling short of the expected criteria of bi-stability for the system to be of use on a practical level.[65, 66] As such, advantage has been taken of a series of previously designed bis-β-diketone ligands, giving access to an elegant way of synthesising polypyrazolyl derivatives. In the case of H_4L, this combines extra potential hydrogen bonding donors in the form of phenol rings, which also provide an additional set of aromatic rings, with a bis(pyrazolyl)pyridyl core. This functionalization of the 3-bpp moiety therefore addresses two of the suggested strategies for the improvement of the cooperativity within SCO systems, namely to favour increased hydrogen bonding, and to induce a greater degree of π-π overlaps.[67] The potential for this ligand to participate in such supramolecular chemistry is witnessed in the resolved crystal structure. The versatility of these ligands has also been shown in the development of several coordination clusters, the formation of which is due to the disposition of the donor atoms and form of the chelating species.

3.10 References

1. J. Klingele, S. Dechert and F. Meyer, *Coord. Chem. Rev.*, 2009, **253**, 2698-2741.
2. M. A. Halcrow, *Dalton Trans.*, 2009, 2059-2073.
3. N. Planas, G. Christian, S. Roeser, E. Mas-Marza, M.-R. Kollipara, J. Benet-Buchholz, F. Maseras and A. Llobet, *Inorg. Chem.*, 2012, **51**, 1889-1901.
4. J. Garcia-Anton, R. Bofill, L. Escriche, A. Llobet and X. Sala, *Eur. J. Inorg. Chem.*, 2012, 4775-4789.
5. L. Francas, X. Sala, J. Benet-Buchholz, L. Escriche and A. Llobet, *ChemSusChem*, 2009, **2**, 321-329.
6. Y. B. Zhou and W. Z. Chen, *Organometallics*, 2007, **26**, 2742-2746.
7. J. Fornies, S. Fuertes, A. Martin, V. Sicilia, E. Lalinde and M. T. Moreno, *Chem.-Eur. J.*, 2006, **12**, 8253-8266.
8. S. O. Malinkin, Y. S. Moroz, L. V. Penkova, M. Haukka, A. Szebesczyk, E. Gumienna-Kontecka, V. A. Pavlenko, E. Nordlander, F. Meyer and I. O. Fritsky, *Inorg. Chim. Acta*, 2012, **392**, 322-330.
9. G. N. Newton, T. Onuki, T. Shiga, M. Noguchi, T. Matsumoto, J. S. Mathieson, M. Nihei, M. Nakano, L. Cronin and H. Oshio, *Angew. Chem.- Int. Ed.*, 2011, **50**, 4844-4848.
10. M. Viciano-Chumillas, G. de Ruiter, S. Tanase, J. M. M. Smits, R. de Gelder, I. Mutikainen, U. Turpeinen, L. J. de Jongh and J. Reedijk, *Dalton Trans.*, 2010, **39**, 4991-4998.
11. T. Matsumoto, T. Shiga, M. Noguchi, T. Onuki, G. N. Newton, N. Hoshino, M. Nakano and H. Oshio, *Inorg. Chem.*, 2009, **49**, 368-370.
12. S. Demeshko, G. Leibeling, S. Dechert and F. Meyer, *Dalton Trans.*, 2006, 3458-3465.
13. M. Viciano-Chumillas, S. Tanase, L. J. de Jongh and J. Reedijk, *Eur. J. Inorg. Chem.*, 2010, 3403-3418.
14. M. A. Halcrow, *Coord. Chem. Rev.*, 2009, **253**, 2493-2514.
15. M. A. Halcrow, *Coord. Chem. Rev.*, 2005, **249**, 2880-2908.
16. R. Pritchard, H. Lazar, S. A. Barrett, C. A. Kilner, S. Asthana, C. Carbonera, J.-F. Letard and M. A. Halcrow, *Dalton Trans.*, 2009, 6656-6666.
17. R. Pritchard, C. A. Kilner and M. A. Halcrow, *Chem. Commun.*, 2007, 577-579.
18. V. A. Money, C. Carbonera, J. Elhaik, M. A. Halcrow, J. A. K. Howard and J. F. Létard, *Chem.-Eur. J.*, 2007, **13**, 5503-5514.
19. K. Takahashi, Y. Hasegawa, R. Sakamoto, M. Nishikawa, S. Kume, E. Nishibori and H. Nishihara, *Inorg. Chem.*, 2012, **51**, 5188-5198.
20. M. Nihei, N. Takahashi, H. Nishikawa and H. Oshio, *Dalton Trans.*, 2011, **40**, 2154-2156.
21. M. Nihei, L. Han and H. Oshio, *J. Am. Chem. Soc.*, 2007, **129**, 5312.
22. J. Olguín and S. Brooker, *Coord. Chem. Rev.*, 2011, **255**, 203-240.
23. E. Coronado, J. C. Dias, M. C. Giménez-López, C. Giménez-Saiz and C. J. Gómez-Garcia, *J. Mol. Struct.*, 2008, **890**, 215-220.
24. K. H. Sugiyarto, W. A. McHale, D. C. Craig, A. D. Rae, M. L. Scudder and H. A. Goodwin, *Dalton Trans.*, 2003, 2443-2448.
25. K. H. Sugiyarto, D. C. Craig, A. D. Rae and H. A. Goodwin, *Aust. J. Chem.*, 1994, **47**, 869-890.
26. K. H. Sugiyarto, M. L. Scudder, D. C. Craig and H. A. Goodwin, *Aust. J. Chem.*, 2000, **53**, 755-765.

27. T. D. Roberts, F. Tuna, T. L. Malkin, C. A. Kilner and M. A. Halcrow, *Chem. Sci.*, 2012, **3**, 349-354.
28. S. A. Barrett, C. A. Kilner and M. A. Halcrow, *Dalton Trans.*, 2011, 12021-12024.
29. S. Marcén, L. Lecren, L. Capes, H. A. Goodwin and J.-F. Létard, *Chem. Phys. Lett.*, 2002, **358**, 87-95.
30. K. H. Sugiyarto and H. A. Goodwin, *Aust. J. Chem.*, 1988, **41**, 1645-1663.
31. K. H. Sugiyarto, K. Weitzner, D. C. Craig and H. A. Goodwin, *Aust. J. Chem.*, 1997, **50**, 869-873.
32. T. Buchen, P. Gütlich, K. H. Sugiyarto and H. A. Goodwin, *Chem.-Eur J.*, 1996, **2**, 1134-1138.
33. M. L. Scudder, D. C. Craig and H. A. Goodwin, *CrystEngComm*, 2005, **7**, 642-649.
34. J. McMurtrie and I. Dance, *CrystEngComm*, 2005, **7**, 216-229.
35. M. L. Scudder, H. A. Goodwin and I. G. Dance, *New J. Chem.*, 1999, **23**, 695-705.
36. V. A. Money, I. R. Evans, M. A. Halcrow, A. E. Goeta and J. A. K. Howard, *Chem. Commun.*, 2003, 158-159.
37. J. M. Holland, J. A. McAllister, C. A. Kilner, M. Thornton-Pett, A. J. Bridgeman and M. A. Halcrow, *J. Chem. Soc. Dalton Trans.*, 2002, 548-554.
38. J. Elhaik, D. J. Evans, C. A. Kilner and M. A. Halcrow, *Dalton Trans.*, 2005, 1693-1700.
39. J. K. McCusker, A. L. Rheingold and D. N. Hendrickson, *Inorg. Chem.*, 1996, **35**, 2100-2112.
40. M. G. B. Drew, C. J. Harding, V. McKee, G. G. Morgan and J. Nelson, *J. Chem. Soc., Chem. Commun.*, 1995, 1035-1038.
41. M. Marchivie, P. Guionneau, J. F. Letard and D. Chasseau, *Acta Cryst. B*, 2003, **59**, 479-486.
42. O. V. Dolomanov, L. J. Bourhis, R. J. Gildea, J. A. K. Howard and H. Puschmann, *J. Appl. Cryst.*, 2009, **42**, 339-341.
43. A. Hauser, *Top. Curr. Chem.*, 2004, **233**, 49-58.
44. M. A. Halcrow, *Chem. Soc. Rev.*, 2011, **40**, 4119-4142.
45. P. Guionneau, M. Marchivie, G. Bravic, J.-F. Létard and D. Chasseau, *Top. Curr. Chem.*, 2004, **234**, 97-128.
46. O. Kahn, *Molecular Magnetism, Wiley VCH*, 1993.
47. P. Gütlich, Y. Garcia and H. A. Goodwin, *Chem. Soc. Rev.*, 2000, **29**, 419-427.
48. M. A. Halcrow, *Chem. Soc. Rev.*, 2008, **37**, 278-289.
49. M. Sorai, *Top. Curr. Chem.*, 2004, **235**, 153-170.
50. M. Sorai, Y. Nakazawa, M. Nakano and Y. Miyazaki, *Chem. Rev.*, 2013, **113**, 41-122.
51. L. A. Barrios, G. Aromí, J. Ribas, J. Salinas Uber, O. Roubeau, K. Sakai, S. Masaoka, P. Gamez and J. Reedijk, *Eur. J. Inorg. Chem.*, 2008, **2008**, 3871-3876.
52. G. Aromí, P. Gamez and J. Reedijk, *Coord. Chem. Rev.*, 2008, **252**, 964-989.
53. R. E. P. Winpenny, *J. Chem. Soc.-Dalton Trans.*, 2002, 1-10.
54. L. A. Barrios, D. Aguilà, O. Roubeau, P. Gamez, J. Ribas-Ariño, S. J. Teat and G. Aromí, *Chem.–Eur. J.*, 2009, **15**, 11235-11243.
55. D. Aguilà, L. A. Barrios, O. Roubeau, S. J. Teat and G. Aromí, *Chem. Commun.*, 2011, **47**, 707-709.
56. E. C. Sañudo, T. Cauchy, E. Ruiz, R. H. Laye, O. Roubeau, S. J. Teat and G. Aromí, *Inorg. Chem.*, 2007, **46**, 9045-9047.

57. T. Jozak, D. Zabel, A. Schubert, Y. Sun and W. R. Thiel, *Eur. J. Inorg. Chem.*, 2010, 5135-5145.
58. B. Zhao, H.-M. Shu, H.-M. Hu, T. Qin and X.-L. Chen, *J. Coord. Chem.*, 2009, **62**, 1025-1034.
59. D. Zabel, A. Schubert, G. Wolmershaeuser, R. L. Jones, Jr. and W. R. Thiel, *Eur. J. Inorg. Chem.*, 2008, 3648-3654.
60. G. Aromí, C. Boldron, P. Gamez, O. Roubeau, H. Kooijman, A. L. Spek, H. Stoeckli-Evans, J. Ribas and J. Reedijk, *Dalton Trans.*, 2004, 3586-3592.
61. G. Aromí, *Comments Inorganic Chem.*, 2011, **32**, 163-194.
62. L. A. Barrios, D. Aguila, O. Roubeau, K. S. Murray and G. Aromí, *Aust. J. Chem.*, 2009, **62**, 1130-1136.
63. G. Aromí, H. Stoeckli-Evans, S. J. Teat, J. Cano and J. Ribas, *J. Mater. Chem.*, 2006, **16**, 2635-2644.
64. G. Aromí, D. Aguilà, P. Gamez, F. Luis and O. Roubeau, *Chem. Soc. Rev.*, 2012, **41**, 537-546.
65. P. Gamez, J. S. Costa, M. Quesada and G. Aromí, *Dalton Trans.*, 2009, 7845-7853.
66. J. F. Létard, P. Guionneau and L. Goux-Capes, *Top. Curr. Chem.*, 2004, **235**, 221-249.
67. P. Gütlich and H. A. Goodwin, *Top. Curr. Chem.*, 2004, **233**, 1-47.